

# Asteroseismology of the pulsating extremely low-mass white dwarf SDSS J111215.82+111745.0: a model with $p$ -mode pulsations consistent with the observations

JIE SU (苏杰) <sup>1,2</sup> AND YAN LI (李焱) <sup>1,2,3,4</sup>

<sup>1</sup>*Yunnan Observatories, Chinese Academy of Sciences, Kunming 650216, People's Republic of China*

<sup>2</sup>*Key Laboratory for the Structure and Evolution of Celestial Objects, Chinese Academy of Sciences, Kunming 650216, People's Republic of China*

<sup>3</sup>*Center for Astronomical Mega-Science, Chinese Academy of Sciences, Beijing 100012, People's Republic of China*

<sup>4</sup>*University of Chinese Academy of Sciences, Beijing 100049, People's Republic of China*

## ABSTRACT

SDSS J111215.82+111745.0 is the second pulsating extremely low-mass white dwarf discovered. Two short-period pulsations, 107.56 and 134.275 s, were detected on this star, which would be the first observed pressure mode ( $p$ -mode) pulsations observed on a white dwarf. While the two potential  $p$ -modes have yet to be confirmed, they make SDSS J111215.82+111745.0 an interesting object. In this work, we analyzed the whole set of seven periods observed on SDSS J111215.82+111745.0. We adopt three independent period-spacing tests to reveal a roughly 93.4 s mean period spacing of  $\ell = 1$   $g$ -modes, which gives added credence to the  $\ell = 1$  identifications. Then we perform asteroseismic modeling for this star, in which the H chemical profile is taken as a variable. The stellar parameters  $M = 0.1650 \pm 0.0137 M_{\odot}$  and  $T_{\text{eff}} = 9750 \pm 560$  K are determined from the best-fit model and the H/He chemical profiles are also defined. The two suspected  $p$ -modes are also well repre-

sented in the best-fit model, and both the stellar parameters and the pulsation frequencies are in good agreement with the values derived from spectroscopy.

*Keywords:* White dwarf stars (1799); Asteroseismology (73); Stellar pulsations (1625); Pulsation modes (1309)

## 1. INTRODUCTION

White dwarf (WD) stars are the final evolutionary stage of the majority of stars in the Galaxy. They thus present an important boundary condition for investigating the previous evolution of stars. In particular, WDs are natural laboratories for studying physical processes under extreme conditions (Winget & Kepler 2008; Fontaine & Brassard 2008; Althaus et al. 2010). WDs with  $M \lesssim 0.45 M_{\odot}$  are classified as low-mass WDs, which are thought to have helium cores. There is a subclass of low-mass WDs called extremely low-mass (ELM) WDs. They are characterized by very low masses, i.e.  $M \lesssim 0.2 M_{\odot}$ . It is widely accepted that ELM WDs are originated from the evolution of close binary systems. The interaction between binary stars removes most of the outer envelope of one component before helium ignition. The remnant of the component with a helium core would not go through the asymptotic giant branch phase and would directly contract toward a WD (see Althaus et al. 2013; Istrate et al. 2016; Li et al. 2019, for instance).

Some ELM WDs have been detected to exhibit pulsations (for example, Hermes et al. 2012, 2013a,b; Kilic et al. 2015; Bell et al. 2015, 2017; Pelisoli et al. 2018). They constitute a separate class of pulsating WDs, commonly referred to as extremely low-mass variables (ELMVs). Pulsations observed in ELMVs are non-radial  $g$ -modes (gravity modes), which are excited by the same mechanism as the classical ZZ Ceti stars, that a combination of the  $\kappa$ - $\gamma$  mechanism (Dolez & Vauclair 1981) and convective driving mechanism (Brickhill 1991). They provide a unique opportunity to explore the invisible interior of ELM WDs by analysing pulsation modes and matching them with theoretical models to obtain information about their chemical composition and structure, to determine their stellar parameters (mass, effective temperature, rotation period, etc.), and to test the scenarios of

their formation by employing asteroseismic tools (Winget & Kepler 2008; Fontaine & Brassard 2008; Althaus et al. 2010).

SDSS J111215.82+111745.0 (hereafter referred to as J1112) was originally discovered to be an ELMV by Hermes et al. (2013a). Seven pulsation modes were detected on J1112, two of which with very short periods (107.56 and 134.275 s), and are suspected to be  $p$ -modes (pressure modes). Theoretical calculations have predicted long ago that  $p$ -mode pulsations can be excited on WDs (see Saio et al. 1983; Starrfield et al. 1983; Hansen et al. 1985; Kawaler 1993, for example). However, the typical periods of  $p$ -modes are comparable to the dynamic time scale  $\tau_{\text{dyn}} \propto 1/\sqrt{\bar{\rho}}$ , which are usually in the order of seconds or less on canonical C/O-core WDs, making it a challenge to detect these pulsation modes. There have been several observational efforts to search for  $p$ -mode pulsations in WDs (e.g. Robinson 1984; Kawaler et al. 1994; Silvotti et al. 2011; Chang et al. 2013; Kilkenny et al. 2014), even with sufficient time resolution (hundreds of milliseconds or even shorter), but no convincing  $p$ -mode pulsation has ever been observed in a pulsating WD. It is most likely the very high surface gravity of a WD makes the amplitudes of  $p$ -modes, which are primarily vertical displacements, too small to be detected. In fact, bona fide  $p$ -mode pulsations have been detected on ELM WD precursors (pre-ELM WDs, see Gianninas et al. 2016, for example). These pre-ELM WDs are quite similar in structure to ELM WDs but have lower surface gravities. The discovery of short-period pulsation on J1112 seems to be the first time that these elusive pulsations have been detected on a WD and need to be confirmed. It makes J1112 an interesting object. On one hand, these  $p$ -modes provide stronger constraints in a complementary way with the existing  $g$ -modes to probe the interior of ELM WDs. On the other hand, we hope to provide a strong support for the confirmation of these suspected  $p$ -modes through modeling and analysis. It is worth mentioning that some previous asteroseismic analysis of J1112 have experimentally taken the potential  $p$ -mode pulsations into account. The work of Córscico & Althaus (2014) is an earlier attempt to fit the two short-period pulsations in J1112 with  $p$ -modes. Their results suggest that if J1112 has a lower mass ( $M \approx 0.16 M_{\odot}$ ) than estimated by spectroscopy ( $M = 0.179 \pm 0.0012 M_{\odot}$ , derived using the models of Althaus et al. 2013), the short-period pulsations (107.56 and 134.275 s) might be interpreted as

low order  $p$ -modes. Another work from [Calcaferro et al. \(2017\)](#) performed period fit to all the seven periods as one case of their analysis.

The paper is organized as follows. Section 2 describes the process of identification of the observed pulsation modes of J1112. A detailed introduction to the modeling for J1112 is presented in Section 3. Section 3.1 describes the theoretical models and Section 3.2 introduces the method for determining the best-fit model and discusses the results. The conclusions are given in Section 4.

## 2. IDENTIFICATION OF THE OBSERVED PULSATION MODES

An important step before doing asteroseismic analysis is to identify the spherical harmonic degree  $\ell$  of the observed pulsation modes. The asymptotic analysis shows that the periods of high-order  $g$ -modes with the same degree  $\ell$  and consecutive radial order  $n$  are expected to have approximately equal spacing ([Tassoul 1980](#)), i.e.

$$\Pi_\ell = P_{\ell,n+1} - P_{\ell,n} \approx \frac{2\pi^2}{\sqrt{\ell(\ell+1)}} \left( \int_0^R \frac{N}{r} dr \right)^{-1}, \quad (1)$$

where  $P_{\ell,n}$  represents the period of pulsation mode with  $\ell$  and  $n$ , and  $N$  is the Brunt-Väisälä frequency. Finding out a constant period spacing from the observed data will help to determine the  $\ell$  value. Three independent methods are used to search for the equal period spacing, namely the K-S test (KST, see [Kawaler 1988](#)), the inverse variance test (IVT, see [O'Donoghue 1994](#)), and the Fourier transform test (FTT, see [Handler et al. 1997](#)). There are seven pulsation modes detected on J1112 ([Hermes et al. 2013a](#)). We perform analysis on the five long periods (1792.905, 1884.599, 2258.528, 2539.695 and 2855.728 s), excluding the two suspected  $p$ -modes (107.56 and 134.275 s). The results are shown in the left panel of Figure 1. In the KST, the minimum value of  $\log Q$  means a uniform period spacing is significant. In the IVT, the maximum value of the inverse variance represents a period spacing with high probability. Similarly, in the FTT, the peak in the square of amplitude ( $|A|^2$ ) indicates a possible period spacing. As shown in the figure, all three tests fail to give a clear period spacing for the five periods. The reason is probably that these periods belong to different  $\ell$ , thus exhibiting inconsistent period spacing. If the period 2855.728 s is eliminated, a clear and significant period spacing at  $\Pi \approx 93.4$  s appears simultaneously in the three tests, as shown in the right



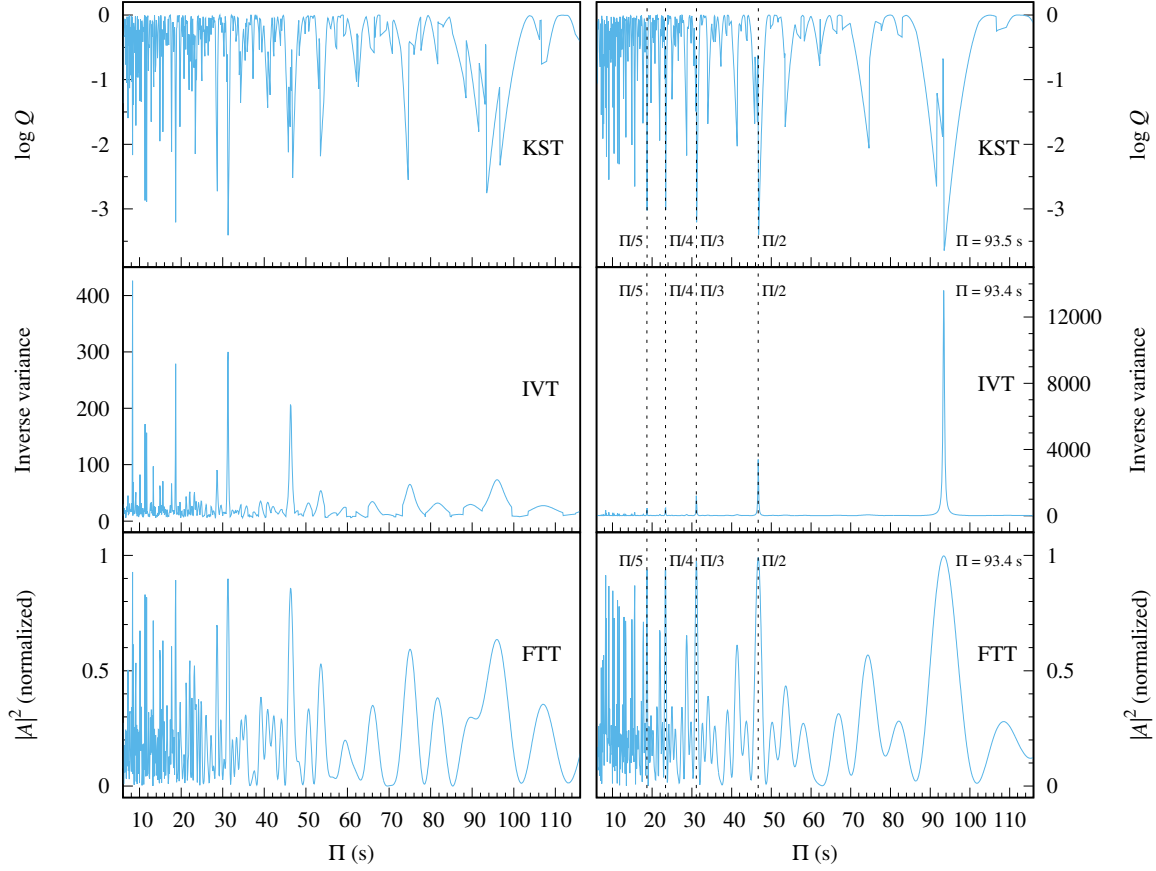


**Figure 1.** The left panels display the results of three independent tests KST, IVT and FTT applied to periods of five  $g$ -modes (1792.905, 1884.599, 2258.528, 2539.695 and 2855.728 s) to search for equal period spacing. The right panels are the same as the left panels, but the results of eliminating the period 2855.728 s. A clear and significant period spacing at  $\Pi \approx 93.4$  s is exhibited simultaneously in the three tests. The vertical dashed lines in right panels indicate the harmonics of the main period spacing ( $\Pi/2$ ,  $\Pi/3$ ,  $\Pi/4$  and  $\Pi/5$ ).

panel of Figure 1. It provides reliable evidence that the four periods (1792.905, 1884.599, 2258.528, and 2539.695 s) belong to the same  $\ell$ . According to [Córscico & Althaus \(2014\)](#), if  $\Pi \approx 93.4$  s is the asymptotic period spacing of  $\ell = 1$   $g$ -modes, the mass of the considered WD is expected to be approximately 0.16 to 0.17  $M_{\odot}$ , which is exactly consistent with the mass ( $M \approx 0.17 M_{\odot}$ ) estimated by [Hermes et al. \(2013a\)](#) from spectroscopy. The above four periods can therefore be identified as  $\ell = 1$  modes. The period 2855.728 s should have a different  $\ell$  value. It may be assumed to be an  $\ell = 2$  mode. Higher  $\ell$  values are unrealistic, because geometrical cancellation makes  $\ell > 2$  modes hard to observe photometrically ([Robinson et al. 1982](#)).

### 3. MODELING

#### 3.1. Theoretical models

In this work, we consider models with parametrized chemical profiles. The scheme of parametrizing chemical composition of WDs had been applied in several previous works (see [Pech et al. 2006](#); [Pech & Vauclair 2006](#); [Bischoff-Kim et al. 2008](#); [Castanheira & Kepler 2008, 2009](#); [Giammichele et al. 2016, 2017, 2018](#); [Lin et al. 2021](#), for instance). We adopt a scheme based on Akima splines ([Akima 1970](#)) to imitate the H abundance profile of the H/He transition zone. A similar scheme was used in the works of [Giammichele et al. \(2017, 2018\)](#) to describe the core chemical profiles of C/O-core WDs. It has been proven to improve the accuracy of modeling. The parameterization scheme is illustrated in [Figure 2](#). As shown in the figure, three control points ( $p_1$ ,  $p_m$  and  $p_2$ ) defined by five parameters are introduced to determine the H/He transition zone, and the parameters are

1.  $q_c$  indicates the location of  $p_1$ , the core boundary,
2.  $c_1$  represents the H abundance ( $X_H$ ) of the core,
3.  $c_2$  represents  $X_H$  of the outer layer,
4.  $t_1$  controls the scale of transition zone below the midpoint ( $p_m$ ), and
5.  $t_2$  controls the scale of transition zone above  $p_m$ ,

where  $p_m$  is defined as the position where  $X_H$  is always equal to  $\frac{1}{2}(c_1 + c_2)$ . Here we only consider H atmosphere WD models with pure He core. Therefore, the two parameters  $c_1$  and  $c_2$  are always fixed as constants, that is  $c_1 = 0$  and  $c_2 = 1$ . There are only three free parameters  $q_c$ ,  $t_1$  and  $t_2$  then can be adjusted. The helium profile is given by  $X_{He} = 1 - X_H$ .

The models for asteroseismic analysis are calculated using the Modules for Experiments in Stellar Astrophysics (MESA, version number 12778), which is a suite of open source libraries for a wide range of applications in stellar astrophysics (see [Paxton et al. 2011, 2013, 2015, 2018, 2019](#), for details). The OPAL equation of state tables ([Rogers & Nayfonov 2002](#)) are used in this work. Radiative opacities are adopted from OPAL tables ([Iglesias & Rogers 1993, 1996](#)) in the high-temperature region and

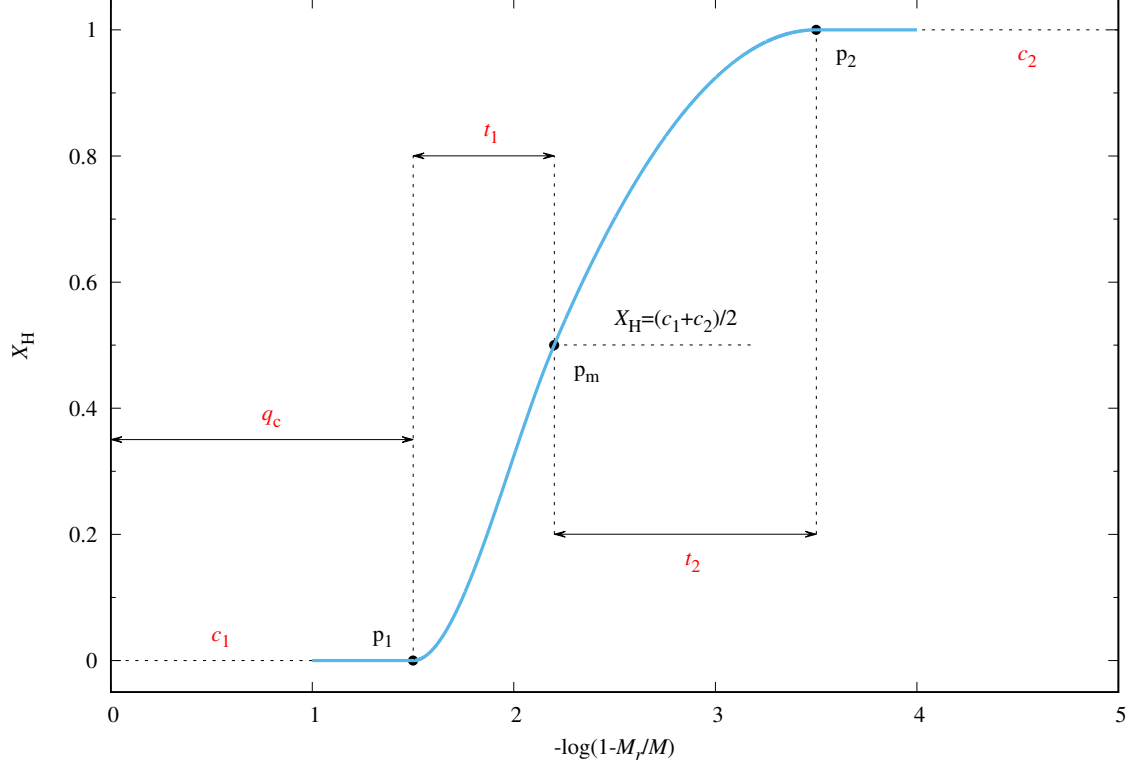


**Figure 2.** Illustration of the parameterization scheme. Three black dots  $p_1$ ,  $p_m$  and  $p_2$  represent control points, which are defined by five parameters. All parameters are labeled in red on the diagram. The control points determine Akima splines (blue curve), which describe the H abundance profile of the H/He transition zone.

tables of [Ferguson et al. \(2005\)](#) in the low-temperature region, the latter include contributions from molecules and grains. Conductive opacities are taken from [Cassisi et al. \(2007\)](#). The nuclear reaction network used is the MESA default `basic.net` that contains eight isotopes:  $^1\text{H}$ ,  $^3\text{He}$ ,  $^4\text{He}$ ,  $^{12}\text{C}$ ,  $^{14}\text{N}$ ,  $^{16}\text{O}$ ,  $^{20}\text{Ne}$ , and  $^{24}\text{Mg}$ . We set the metal composition as the abundance ratio of GS98 ([Grevesse & Sauval 1998](#)). The mixing length theory (MLT) formulation of [Bohm & Cassinelli \(1971\)](#) is employed to deal with convection. The mixing length parameter is set to  $\alpha_{\text{MLT}} = 2$  (MESA default setting) during the evolution of WD progenitor, and  $\alpha_{\text{MLT}} = 0.6$  during the evolution of WD, which refers to the value recommended by [Bergeron et al. \(1995\)](#). We include element diffusion in our models using the scheme described by [Thoul et al. \(1994\)](#), but ignore convective overshoot and rotational mixing. It is worth mentioning that rotation plays a critical role in determining the structure of ELM WD

as well as diffusion (Istrate et al. 2016). Ignoring effects such as rotation would lead to inaccurate models. However, introducing parameterized chemical profiles into WD models is expected to reduce some inaccuracies.

The He WD models are generated from the zero-age main sequence (ZAMS) progenitors through stellar evolution. They start with two models with initial masses ( $M_{\text{ini}}$ ) of  $0.8$  and  $0.9 M_{\odot}$ , respectively. All models are assumed to have initial chemical compositions of  $(X, Y, Z) = (0.7, 0.28, 0.02)$ . We evolve the model with  $M_{\text{ini}} = 0.8 M_{\odot}$  until its radius exceeds  $1.5 R_{\odot}$ , and then the mass loss rate is enhanced, allowing a large amount of the envelope to be stripped off before the He flash occurs. For the model with  $M_{\text{ini}} = 0.9 M_{\odot}$ , this process is started when its radius exceeds  $3 R_{\odot}$ . In the subsequent evolution, the model with  $M_{\text{ini}} = 0.9 M_{\odot}$  goes through repeated diffusion-induced CNO flashes (e.g. Althaus et al. 2001; Panei et al. 2007; Althaus et al. 2013; Istrate et al. 2016) and then arrive at the WD cooling track. The evolution is stopped when  $\log(L/L_{\odot}) < -1$  and an initial WD model with mass of  $0.2084 M_{\odot}$  is obtained (hereafter referred to as WD-02084). However, the model with  $M_{\text{ini}} = 0.8 M_{\odot}$  do not experience a similar process of CNO flashes, but directly form a WD with a lower mass of  $0.1789 M_{\odot}$  (hereafter referred to as WD-01789). Figure 3 shows the evolutionary tracks of the two progenitors in the Hertzsprung-Russell (H-R) diagram. An example of the `inlist` options for the model with  $M_{\text{ini}} = 0.8 M_{\odot}$  is listed in Appendix A for reference (the options for the model with  $M_{\text{ini}} = 0.9 M_{\odot}$  are similar). In addition, we made some modifications to the source file `run_star_extras.f` to add custom options. The contents of the modified `run_star_extras.f` file are shown in Appendix B.

The parameterized H/He profiles are calculated separately and incorporated into MESA using the `relax_initial_composition` option to get models with different chemical profiles. An example of the `inlist` for relaxing the composition of a model is shown in Appendix C. The range and step of the profile parameters,  $q_c$ ,  $t_1$  and  $t_2$ , adopted in different grids are listed in Table 1. The mass of a certain model with given chemical profiles is rescaled without changing composition by setting the `relax_mass_scale` option to obtain models with different masses. We relax WD-01789 to create models with masses of  $0.15 \leq M < 0.18 M_{\odot}$  and relax WD-02084 to create WD models with masses

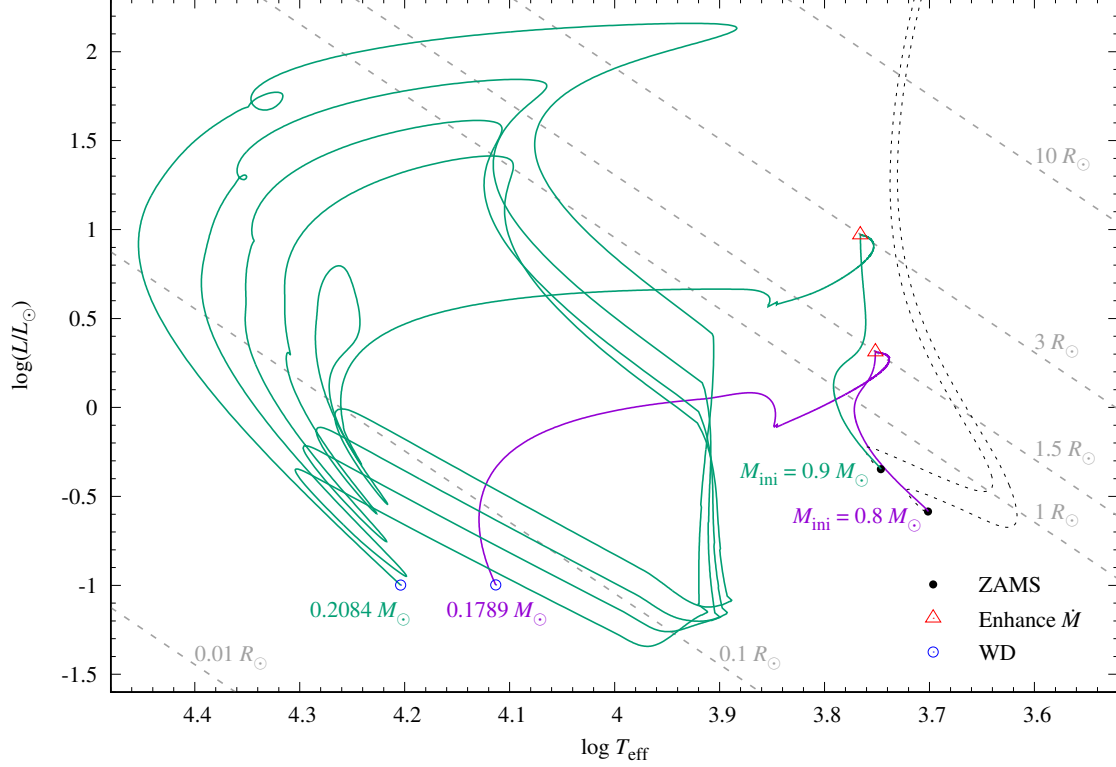


**Figure 3.** The H-R diagram shows the formation of our He WD models. The black dotted lines represent the evolutionary tracks of the pre-main sequence stages and the black points indicate the locations of the zero-age main sequence (ZAMS). The red triangles in the figure indicate the stages where the mass loss rate ( $\dot{M}$ ) are enhanced. It shows that the model with  $M_{\text{ini}} = 0.9 M_{\odot}$  experiences multiple diffusion-induced CNO flashes and finally forms a WD with  $M = 0.2084 M_{\odot}$ . The other model with  $M_{\text{ini}} = 0.8 M_{\odot}$  do not experience a similar process, but directly forms a WD with  $M = 0.1789 M_{\odot}$ . The grey dashed lines in the background represent grid lines corresponding to different  $R_{\odot}$  values.

of  $0.18 \leq M \leq 0.2$ . The model grid used for this analysis covers the range in  $M$  from  $0.15$  to  $0.2 M_{\odot}$  in step of  $0.001$  (coarse grid) and  $0.0001 M_{\odot}$  (fine grid), and  $T_{\text{eff}}$  from  $7000$  to  $12000$  K. An example of the `inlist` for relaxing the mass of a model and cooling it are shown in Appendix D. The stellar oscillation code `GYRE` (Townsend & Teitler 2013) is adopted to calculate the eigenfrequencies and eigenfunctions of the oscillation modes of each model in the grid. The Brunt-Väisälä frequency from the model is smoothed by the built-in weighted smoothing in `MESA` using two cells on either side (`MESA` default setting), in order to reduce the influence of numerical noise on theoretical frequencies.

**Table 1.** The minimum (Min.), maximum (Max.) and step values of the profile parameters,  $q_c$ ,  $t_1$  and  $t_2$ , adopted in four grids with different resolutions.

|        | $q_c$ |      |       | $t_1$ |      |       | $t_2$ |      |       |
|--------|-------|------|-------|-------|------|-------|-------|------|-------|
|        | Min.  | Max. | Step  | Min.  | Max. | Step  | Min.  | Max. | Step  |
| Grid 1 | 0.30  | 0.80 | 0.1   | 0.50  | 1.50 | 0.1   | 0.50  | 1.50 | 0.1   |
| Grid 2 | 0.30  | 0.50 | 0.05  | 0.60  | 0.80 | 0.05  | 1.20  | 1.40 | 0.05  |
| Grid 3 | 0.35  | 0.45 | 0.01  | 0.65  | 0.75 | 0.01  | 1.30  | 1.40 | 0.01  |
| Grid 4 | 0.39  | 0.41 | 0.001 | 0.68  | 0.70 | 0.001 | 1.33  | 1.35 | 0.001 |

### 3.2. Asteroseismic analysis

The analysis is based on the forward modeling approach, which involves finding the best match between a set of oscillation frequencies detected in a given star and the frequencies calculated from the models. The goodness of matching for each model is quantified by a merit function defined as

$$S^2 \equiv \frac{1}{N} \sum_{i=1}^N [f_O(i) - f_T]^2, \quad (2)$$

where  $f_O(i)$  is the frequency of the  $i$ -th observed mode,  $f_T$  is the theoretical frequency which is the closest one to  $f_O(i)$ , and  $N = 7$  is the total number of observed modes. The model with minimum  $S^2$  is considered to be the best-fit model. In Section 2, four of the observed  $g$ -modes (557.7542, 530.6170, 442.7662 and 393.7480  $\mu\text{Hz}$ ) are identified to be  $\ell = 1$  modes and the other one (350.1734  $\mu\text{Hz}$ ) to be  $\ell = 2$  mode. Each of them only needs to match the theoretical frequency of the corresponding  $\ell$  value. As for the two suspected  $p$ -modes (7447.388 and 9297.4  $\mu\text{Hz}$ ), due to the lack of clear identification of their  $\ell$  values, each of them will match the theoretical frequency of  $\ell = 0, 1$ , and 2, respectively. ELM WDs are expected to be relatively rapidly rotating (e.g. [Istrate et al. 2016](#)). Thus, rotational splittings are expected to be observed in all the non-radial pulsation modes. However, no triplet or quintet produced by rotational splitting was observed among the seven observed modes. We assumed

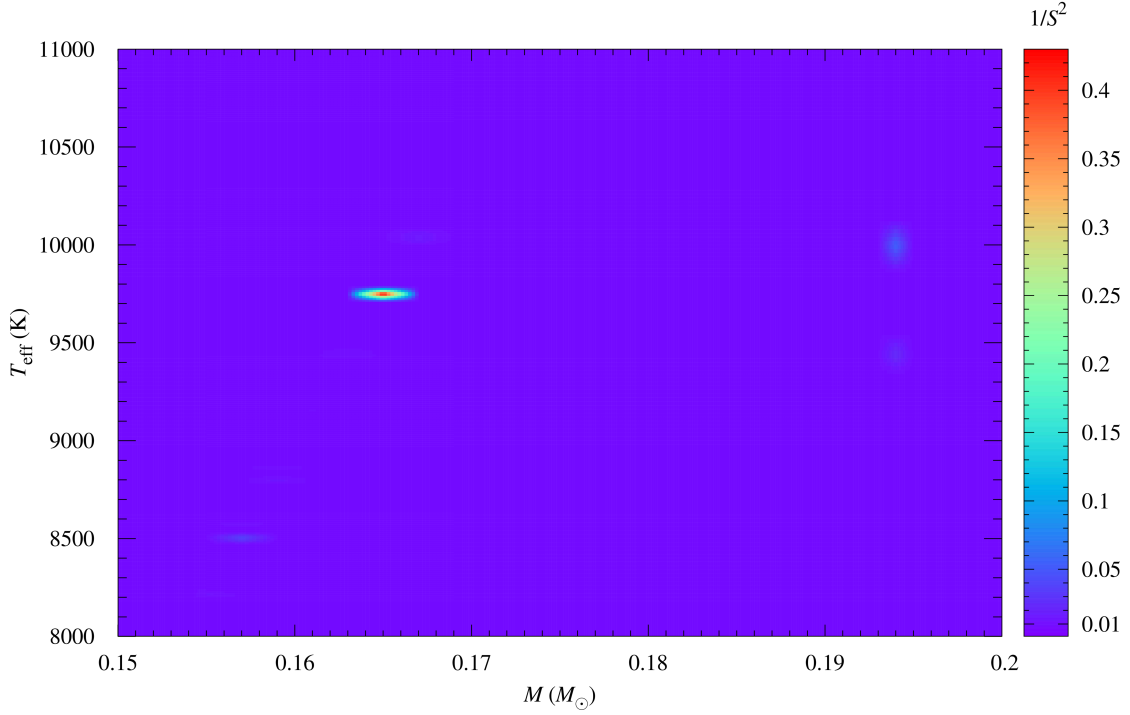


**Figure 4.** The heat map shows the projection of  $1/S^2$  on the  $M$  versus  $T_{\text{eff}}$  plane. The best-fit model is located at  $M = 0.1650 M_{\odot}$  and  $T_{\text{eff}} = 9750 \text{ K}$ , which corresponds to the maximum of  $1/S^2 \approx 0.423$  ( $S^2 \approx 2.366$ ).

implicitly that all observed modes are  $m = 0$ , because there is not enough evidence to confirm their  $m$  values. Therefore, we only explore the theoretical modes of  $m = 0$ , and do not consider rotational multiplets. However, this assumption is somewhat suspicious. We should be aware that this would bring some uncertainties to the results.

We find out the best-fit model with a minimum  $S^2$  of 2.366. The mass and effective temperature of the best-fit model are  $M = 0.1650 M_{\odot}$  and  $T_{\text{eff}} = 9750 \text{ K}$ . The parameters characterizing its H chemical profile are  $q_c = 0.399$ ,  $t_1 = 0.685$  and  $t_2 = 1.343$ , which correspond to an H envelope mass of  $\log(M_{\text{H}}/M) = -1.45$ . Figure 4 shows the projection of the inverse of the merit function,  $1/S^2$ , on the  $M$  versus  $T_{\text{eff}}$  plane with the chemical profiles to be fixed as the best-fit solution. Figure 5 shows  $1/S^2$  varies with the H chemical profile when  $M$  and  $T_{\text{eff}}$  are fixed, where the H chemical profile of the best-fit model is fine tuned and the value of  $1/S^2$  is indicated by the color scale.

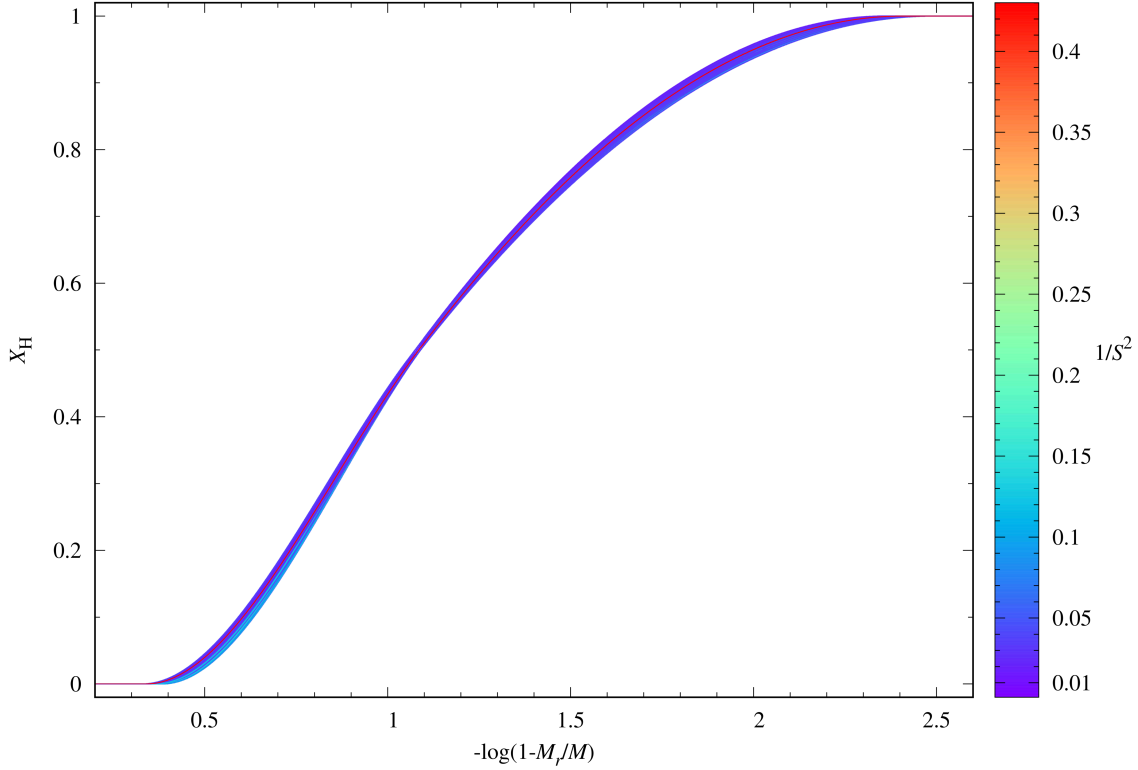


**Figure 5.** The variation of  $1/S^2$  when  $M$  and  $T_{\text{eff}}$  are fixed and the H chemical profile of the best-fit model is fine tuned. The value of  $1/S^2$  is indicated by the color scale.

We use the bootstrap method (Efron 1979) to estimate the uncertainties of  $M$  and  $T_{\text{eff}}$  of the best-fit model. The bootstrap is a Monte Carlo simulation based on a large number of synthetic data sets that sampled from the original data set. The size of each synthetic data set must be equal to the size of the original data set. First, we sample seven data points at a time with replacement from the seven observed frequencies to form a new data set (called bootstrap sample). To account for the perturbation of each frequency by its observational uncertainty ( $\sigma_f$ ), a normally distributed random noise with zero mean and standard deviation  $\sigma_f$  is added to each sample point. Then the bootstrap sample is taken to match the models to obtain parameters with the minimum  $S^2$ . The fitted parameters obtained in this way are expressed as simulated parameters ( $M^s$  and  $T_{\text{eff}}^s$ ). This procedure is repeated 50000 times in this work. The distribution of these  $M^s$  and  $T_{\text{eff}}^s$  around the best-fit parameters  $M^* = 0.1650 M_{\odot}$  and  $T_{\text{eff}}^* = 9750 \text{ K}$  is then analyzed. Histograms of the distribution of  $M^s - M^*$  and  $T_{\text{eff}}^s - T_{\text{eff}}^*$  are shown in the upper panels of Figure 6. We fit each



histogram with a Gaussian function and get the standard deviation ( $\sigma$ ) from the fitting curve. It gives  $\sigma \approx 0.0045 M_{\odot}$  for mass and  $\sigma \approx 250$  K for effective temperature. However,  $\sigma_f$  is generally less than  $0.002 \mu\text{Hz}$ , which is several orders of magnitude smaller than the frequency difference between the observed and theoretical frequencies ( $|f_T - f_O|$ , see Table 3). In order to accommodate the large mismatch between the observed modes compared to the theoretical ones, we try to introduce normally distributed random noise with standard deviation  $|f_T - f_O|$  to perform bootstrapping analysis again. The distributions of  $M^s - M^*$  and  $T_{\text{eff}}^s - T_{\text{eff}}^*$  along with the corresponding fitting curve are shown in the lower panels of Figure 6. The results for this case are  $\sigma \approx 0.0056 M_{\odot}$  for mass and  $\sigma \approx 410$  K for effective temperature.

We can also estimate the distance to J1112 by using the luminosity of the best-fit model ( $L = 0.067624 L_{\odot}$ ) and the Gaia apparent magnitude of J1112 ( $G = 16.335$  mag), which is similar to what Lopez et al. (2021) has done recently. We use the 3D reddening map of Green et al. (2018) and apply the  $R_V = 3.1$  reddening law of Fitzpatrick (1999) to obtain the extinction of  $A_V = 0.073$ . We then use the bolometric correction of Choi et al. (2016) for a star with  $T_{\text{eff}} = 9750$  K,  $\log g = 6.0$  and  $A_V = 0.1$  to determine the seismic distance of 434.3 pc. However, this value deviates significantly from the parallax distance determined from Gaia eDR3 of  $361.4^{+6.5}_{-7.7}$  pc (Bailer-Jones et al. 2021), which suggests that the luminosity of our model is greater than that measured by Gaia parallax. If we assume that the seismic distance of our model agrees with the parallax distance at the  $1-\sigma$  level, the seismic distance should be estimated to be  $434.3 \pm 66.4$  pc. In order to be consistent with the uncertainty of this distance, the luminosity of our model should lie in the range of  $0.048526$  to  $0.089881 L_{\odot}$ . We try to use the variance of luminosity to estimate the uncertainties of our model parameters, which gives  $\sigma \approx 0.0137 M_{\odot}$  for mass and  $\sigma \approx 560$  K for effective temperature. It suggests that the uncertainties of mass and effective temperature derived from bootstrap simulations are somewhat underestimated. Based on the above analysis, we will choose the uncertainties estimated by the last scheme as the final results, i.e.  $M = 0.1650 \pm 0.0137 M_{\odot}$  and  $T_{\text{eff}} = 9750 \pm 560$  K, which are considered more reliable.

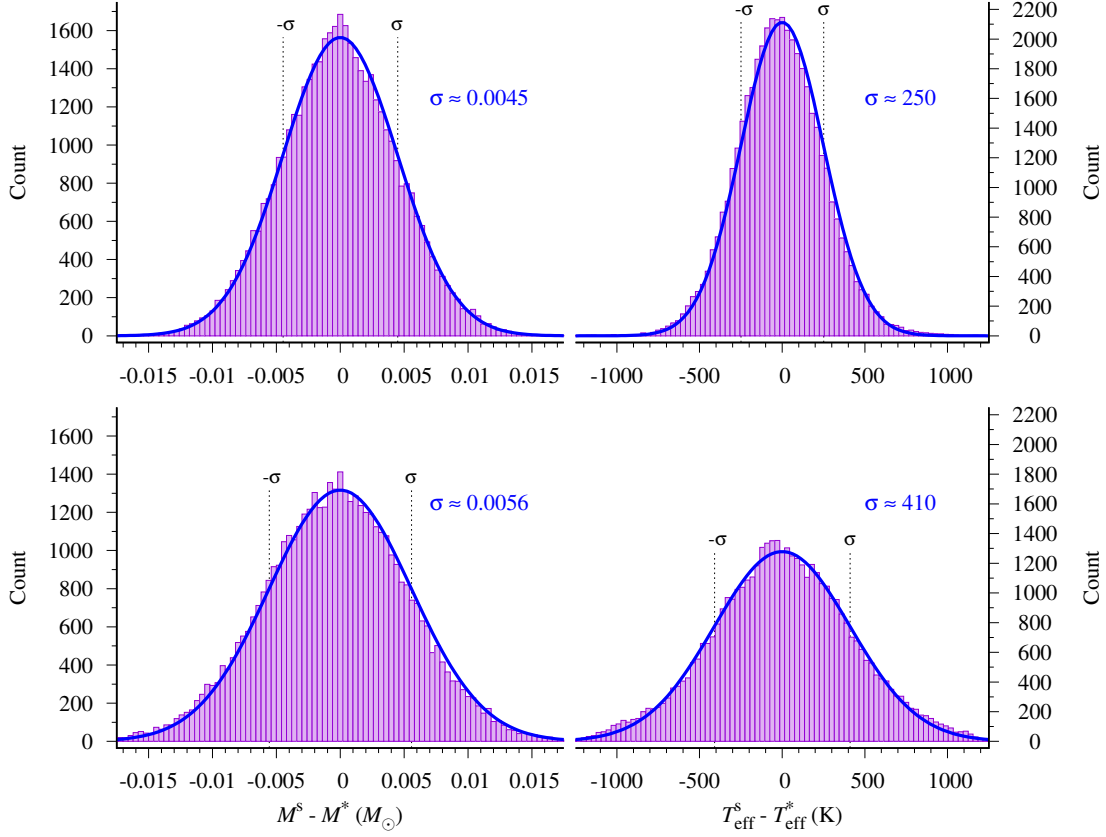


**Figure 6.** Histograms of the distribution of simulated parameters  $M^s$  and  $T_{\text{eff}}^s$  around the best-fit parameters  $M^* = 0.1650 M_\odot$  and  $T_{\text{eff}}^* = 9750 \text{ K}$ . The blue curves are results of fitting the histograms with Gaussian function, from which the standard deviations ( $\sigma$ ) are obtained. The upper panels show the results for the case where the simulated random noises are equivalent to the observational uncertainties, which give  $\sigma \approx 0.0045 M_\odot$  for mass and  $\sigma \approx 250 \text{ K}$  for effective temperature. The lower panels show the results for the case where the simulated random noises correspond to the differences between the observed and theoretical frequencies. The results for this case are  $\sigma \approx 0.0056 M_\odot$  for mass and  $\sigma \approx 410 \text{ K}$  for effective temperature.

The atmospheric parameters of J1112 from spectroscopic measurement were previously published by [Brown et al. \(2012\)](#) and [Hermes et al. \(2013a\)](#). The current values include corrections of [Tremblay et al. \(2015\)](#) for the 3D treatment of convection, i.e.  $T_{\text{eff}} = 9240 \pm 140 \text{ K}$  and  $\log g = 6.17 \pm 0.06$ , which corresponds to a stellar mass of  $0.169 M_\odot$ . The stellar mass and effective temperature of our best-fit model are consistent with the spectroscopic results and the asteroseismic solutions ( $M = 0.1612 M_\odot$  and  $T_{\text{eff}} = 9301 \text{ K}$ ) of [Calcaferro et al. \(2018\)](#) within  $1\text{-}\sigma$  uncertainty. The hydrogen-layer mass ( $M_{\text{H}}/M$ ) of J1112 derived from the present work are slightly greater than the asteroseismic solutions

**Table 2.** Comparison between the stellar parameters obtained in this work and the previous results.

| $M (M_{\odot})$     | $T_{\text{eff}} \text{ (K)}$ | $\log g \text{ (cgs)}$ | $\log (M_{\text{H}}/M)$ | Work                     |
|---------------------|------------------------------|------------------------|-------------------------|--------------------------|
| $0.1650 \pm 0.0137$ | $9750 \pm 560$               | $5.73 \pm 0.15$        | $-1.45$                 | This                     |
| $0.16^a$            | $(9400 \pm 490)^b$           | $(5.81 \pm 0.12)^b$    | -                       | Brown et al. (2012)      |
| $0.17^a$            | $(9590 \pm 140)^b$           | $(6.36 \pm 0.06)^b$    | -                       | Hermes et al. (2013a)    |
| $0.179 \pm 0.0012$  | $(9590 \pm 140)^b$           | $(6.36 \pm 0.06)^b$    | -                       | Althaus et al. (2013)    |
| 0.169               | $9240 \pm 140$               | $6.17 \pm 0.06$        | -                       | Tremblay et al. (2015)   |
| 0.2389              | 9300                         | 6.9215                 | $-2.45$                 | Calcaferro et al. (2017) |
| 0.1612              | 9301                         | 5.9695                 | $-1.76$                 | Calcaferro et al. (2018) |

<sup>a</sup> Estimated using the models of Panei et al. (2007).

<sup>b</sup> Preliminary spectroscopic results without 3D corrections.

of Calcaferro et al. (2017, 2018), i.e.  $\log (M_{\text{H}}/M) = -2.45$  and  $\log (M_{\text{H}}/M) = -1.76$ , respectively. It is worth mentioning that the results of Calcaferro et al. (2018) was based on the five observed  $g$ -modes, but our analysis takes the whole set of (seven) frequencies into account. Moreover, the differences between the two results may reflect some differences between the theoretical models of Calcaferro et al. (2017, 2018) and ours. Moreover, the mass of our best-fit is in agreement with the previous estimates of  $M \approx 0.17 M_{\odot}$  by Hermes et al. (2013a) and  $M = 0.169 M_{\odot}$  by Tremblay et al. (2015). It is also consistent with the suggestion of Córscico & Althaus (2014) that the two short-period pulsations might be caused by low-order  $p$ -modes if the mass of J1112 is  $M \approx 0.16 M_{\odot}$ . A comparison between the stellar parameters obtained in this work and the results of previous work is listed in Table 2.

A part of the theoretical frequencies ( $f_{\text{T}}$ ) of the best-fit model are listed in Table 3 along with their spherical harmonic degree  $\ell$  and radial order  $n$ . The observed frequencies ( $f_{\text{O}}$ ) and the corresponding period and amplitude values are listed beside the matched theoretical frequencies. The absolute

**Table 3.** Comparison of the theoretical and observed frequencies of the best-fit model. The theoretical frequencies  $f_T$  are listed along with their spherical harmonic degree  $\ell$  and radial order  $n$ . The seven observed frequencies  $f_O$  and the corresponding period and amplitude values are listed beside the matched theoretical frequencies. The absolute frequency differences  $|f_T - f_O|$  are also listed.

|            | Theoretical |     |          |                    |                    | Observed (Hermes et al. 2013a) |          |           |
|------------|-------------|-----|----------|--------------------|--------------------|--------------------------------|----------|-----------|
|            | $\ell$      | $n$ | Period   | Frequency          | $ f_T - f_O $      | Frequency                      | Period   | Amplitude |
|            |             |     | (s)      | ( $\mu\text{Hz}$ ) | ( $\mu\text{Hz}$ ) | ( $\mu\text{Hz}$ )             | (s)      | (mma)     |
| $p$ -modes | 1           | 2   | 134.258  | 7448.3354          | 0.9474             | $7447.388 \pm 0.010$           | 134.275  | 0.44      |
|            | 2           | 2   | 107.567  | 9296.5663          | 0.8337             | $9297.4 \pm 3.6$               | 107.56   | 0.38      |
| $g$ -modes | 1           | -17 | 1787.030 | 559.5877           | 1.8335             | $557.7542 \pm 0.0017$          | 1792.905 | 3.31      |
|            | 1           | -18 | 1875.696 | 533.1355           | 2.5185             | $530.6170 \pm 0.0011$          | 1884.599 | 4.73      |
|            | 1           | -22 | 2262.705 | 441.9489           | 0.8173             | $442.7662 \pm 0.0007$          | 2258.528 | 7.49      |
|            | 1           | -25 | 2551.858 | 391.8713           | 1.8767             | $393.7480 \pm 0.0007$          | 2539.695 | 6.77      |
|            | 2           | -50 | 2864.230 | 349.1340           | 1.0394             | $350.1734 \pm 0.0013$          | 2855.728 | 3.63      |
|            |             |     |          |                    |                    |                                |          |           |

frequency differences  $|f_T - f_O|$  are also listed in the table. We hence identify the  $\ell$  and  $n$  values of the seven observed modes. Four observed periods 1792.905, 1884.599, 2258.528, and 2539.695 s (frequencies 557.7542, 530.6170, 442.7662 and 393.7480  $\mu\text{Hz}$ ), have been identified as  $\ell = 1$   $g$ -mode in Section 2, and their  $n$  values are determined as 17, 18, 22 and 25 by comparing them to the theoretical modes. The period 2855.728 s (frequency 350.1734  $\mu\text{Hz}$ ) is identified to be a  $g$ -mode with  $\ell = 2$  and  $n = 50$ . The two suspected  $p$ -mode, 107.56 and 134.275 s (9297.4 and 7447.388  $\mu\text{Hz}$ ), are identified as  $\ell = 2$ ,  $n = 2$  and  $\ell = 1$ ,  $n = 2$ , respectively. It is worth noting that the periods calculated by the best-fit model, 107.567 and 134.258 s, are in excellent agreement with these two observations (107.56 and 134.275 s).

#### 4. CONCLUSIONS

SDSS J111215.82+111745.0 is the second ELMV discovered. Two short-period pulsations were detected on this star, which means that  $p$ -mode pulsations may be observed on WDs for the first time. However, the reality of these two  $p$ -modes has not been definitively confirmed observationally. In this work, we perform a detailed asteroseismic analysis on J1112, taking the whole set of pulsation modes into account. For the five  $g$ -modes, three independent methods are used to help us identify that four of them are  $\ell = 1$  modes and the other is  $\ell = 2$  mode. On this basis, we make asteroseismic modeling for the star, in which the H chemical profile is taken as a variable. The main parameters are determined from the best-fit model and the H/He chemical profiles are defined. The effective temperature and mass of J1112 determined from our model are in good agreement with the parameters derived from spectroscopy and also are compatible with the results of other asteroseismic analysis. It is important that the two suspected  $p$ -modes, 107.56 and 134.275 s (9297.4 and 7447.388  $\mu$ Hz), are well represented in our best-fit model. Both the stellar parameters and the pulsation frequencies are in good agreement with the observations. We have found a model with  $p$ -mode pulsations consistent with the periods observed on J1112, which provides theoretical support for the reality of these two  $p$ -modes.

Further observations are needed in the future. It can be expected that, with the development of observations on more ELMVs, it will be possible to discover more  $p$ -mode pulsations.

We would like to thank an anonymous referee for reviewing and offering valuable comments, which greatly help us to improve the manuscript. This research is supported in part by the National Key R&D Program of China (Grant No. 2021YFA1600400/2021YFA1600402), by the B-type Strategic Priority Program No. XDB41000000 funded by the Chinese Academy of Sciences (CAS), and by the National Natural Science Foundation of China (NSFC) under grants 12133011 and 11833006. This work makes use of the “PHOENIX Supercomputing Platform” jointly operated by the Binary Population Synthesis Group and the Stellar Astrophysics Group at Yunnan Observatories, CAS.

## APPENDIX

## A. AN EXAMPLE OF THE INLIST FOR GENERATING HE WD FROM ZAMS

```

&star_job

  show_log_description_at_start = .false.
  create_pre_main_sequence_model = .true.
  set_uniform_initial_composition = .true.

    initial_h1 = 0.7
    initial_h2 = 0.0
    initial_he3 = 0.0
    initial_he4 = 0.28
    initial_zfracs = 3      !< GS98_zfracs = 3 >
  kappa_file_prefix = 'gs98'
  eos_file_prefix = 'mesa'
  save_photo_when_terminate = .false.
  save_model_when_terminate = .true.
  save_model_filename = 'he_wd.mod'
  write_profile_when_terminate = .true.
  filename_for_profile_when_terminate = 'he_wd_xxxx.dat'

/ ! end of star_job namelist

&controls

  initial_mass = 0.8
  initial_z = 0.02
  atm_option = 'T_tau'
  atm_T_tau_relation = 'Eddington'
  atm_build_tau_outer = 1.0d-6
  MLT_option = 'ML2'
  mixing_length_alpha = 2.0

```

```

cool_wind_RGB_scheme = 'Reimers'

Reimers_scaling_factor = 0.5

do_element_diffusion = .true.

!<-----
! solve the system of equations described by Thoul et al. (1994)
diffusion_use_cgs_solver = .false.

!----->

diffusion_min_dq_at_surface = 1.0d-3
profile_interval = -1
history_interval = 1
terminal_interval = 1
write_header_frequency = 100
write_profiles_flag = .false.
remove_H_wind_H_mass_limit = 1.0d-2

!<-----
! custom option
! enhance the mass loss rate when R/Rsun > this value
x_ctrl(1) = 1.5

!----->

!<-----
! custom stopping condition
! stop when log(L/Lsun) < this value
x_ctrl(2) = -1.d0

!----->

/ ! end of controls namelist

```

## B. MODIFICATIONS TO THE SOURCE FILE 'RUN\_STAR\_EXTRAS.F'

```

module run_star_extras

```

```

use star_lib
use star_def
use const_def
use math_lib
contains

```

```

subroutine extras_controls(id, ierr)
  integer, intent(in) :: id
  integer, intent(out) :: ierr
  type (star_info), pointer :: s
  ierr = 0
  call star_ptr(id, s, ierr)
  if (ierr /= 0) return
  s%extras_check_model => extras_check_model
  s%job%warn_run_star_extras = .false.
end subroutine extras_controls

```

```

integer function extras_check_model(id)
  integer, intent(in) :: id
  integer :: ierr
  type (star_info), pointer :: s
  ierr = 0
  call star_ptr(id, s, ierr)
  if (ierr /= 0) return
  extras_check_model = keep_going
  if (s%center_h1 < 1.0d-10 .and. s%log_surface_radius > log10(s%x_ctrl(1))) &
    s%remove_H_wind_mdot = 1.0d-7

```



```

if (s%center_gamma > 1.0d0 .and. s%log_L_surf < s%x_ctrl(2)) then
    extras_check_model = terminate
    write(*, *) 'have reached desired conditions'
    return
end if

if (extras_check_model == terminate) &
    s%termination_code = t_extras_check_model

end function extras_check_model

end module run_star_extras

```

### C. AN EXAMPLE OF THE INLIST FOR RELAXING THE COMPOSITION OF A MODEL

```

&star_job

    show_log_description_at_start = .false.

    load_saved_model = .true.

    saved_model_name = 'he_wd_xxxx.dat'

    kappa_file_prefix = 'gs98'

    eos_file_prefix = 'mesa'

    relax_initial_composition = .true.

    relax_composition_filename = 'comp_xxxx.dat'

    num_steps_to_relax_composition = 100

    save_model_when_terminate = .true.

    save_model_filename = 'wd_comp_xxxx.mod'

    steps_to_take_before_terminate = 10

/ ! end of star_job namelist

```

```

&controls

    atm_option = 'T_tau'

    atm_T_tau_relation = 'Eddington'

```

```

atm_build_tau_outer = 1.0d-6
mesh_delta_coeff = 0.2
dxdt_nuc_factor = 0.0
eps_nuc_factor = 0.0
mix_factor = 0.0
profile_interval = -1
history_interval = -1
terminal_interval = 1
write_header_frequency = 100
max_years_for_timestep = 1.0
/ ! end of controls namelist

```

#### D. AN EXAMPLE OF THE INLIST FOR RELAXING THE MASS OF A MODEL AND COOLING IT

```

&star_job
  show_log_description_at_start = .false.
  load_saved_model = .true.
  saved_model_name = 'wd_comp_xxxx.mod'
  kappa_file_prefix = 'gs98'
  eos_file_prefix = 'mesa'
  relax_mass_scale = .true.
  new_mass = 0.16      !< new mass = 0.16 Msun, for example >
  dlgm_per_step = 1.0d-3
  change_mass_years_for_dt = 1.0
  set_initial_dt = .true.
  years_for_initial_dt = 1.0
/ ! end of star_job namelist

```

```
&controls

  atm_option = 'T_tau'

  atm_T_tau_relation = 'Eddington'

  atm_build_tau_outer = 1.0d-6

  add_atmosphere_to_pulse_data = .true.

  MLT_option = 'ML2'

  mixing_length_alpha = 0.6      !< recommended by Bergeron et al. (1995) >

  mesh_delta_coeff = 0.2

  profile_interval = 1

  history_interval = 1

  terminal_interval = 1

  write_header_frequency = 100

  max_num_profile_models = -1

  profile_header_include_sys_details = .false.

  write_pulse_data_with_profile = .true.

  pulse_data_format = 'GYRE'

  Teff_lower_limit = 7.0d3

/ ! end of controls namelist
```

## REFERENCES

- |  |  |
|--|--|
| <p>Akima, H. 1970, JACM, 17, 589</p> <p>Althaus, L. G., Córscico, A. H., Isern, J., &amp; García-Berro, E. 2010, A&amp;A Rv, 18, 471</p> <p>Althaus, L. G., Miller Bertolami, M. M., &amp; Córscico, A. H. 2013, A&amp;A, 557, A19</p> <p>Althaus, L. G., Serenelli, A. M., &amp; Benvenuto, O. G. 2001, MNRAS, 323, 471</p> | <p>Bailer-Jones, C. A. L., Rybizki, J., Fouesneau, M., Demleitner, M., &amp; Andrae, R. 2021, AJ, 161, 147</p> <p>Bell, K. J., Kepler, S. O., Montgomery, M. H., et al. 2015, in Astronomical Society of the Pacific Conference Series, Vol. 493, 19th European Workshop on White Dwarfs, ed. P. Dufour, P. Bergeron, &amp; G. Fontaine, 217</p> |
|--|--|

- Bell, K. J., Gianninas, A., Hermes, J. J., et al. 2017, *ApJ*, 835, 180
- Bergeron, P., Wesemael, F., Lamontagne, R., et al. 1995, *ApJ*, 449, 258
- Bischoff-Kim, A., Montgomery, M. H., & Winget, D. E. 2008, *ApJ*, 675, 1505
- Bohm, K. H., & Cassinelli, J. 1971, *A&A*, 12, 21
- Brickhill, A. J. 1991, *MNRAS*, 251, 673
- Brown, W. R., Kilic, M., Allende Prieto, C., & Kenyon, S. J. 2012, *ApJ*, 744, 142
- Calcaferro, L. M., Córscico, A. H., & Althaus, L. G. 2017, *A&A*, 607, A33
- Calcaferro, L. M., Córscico, A. H., Althaus, L. G., Romero, A. D., & Kepler, S. O. 2018, *A&A*, 620, A196
- Cassisi, S., Potekhin, A. Y., Pietrinferni, A., Catelan, M., & Salaris, M. 2007, *ApJ*, 661, 1094
- Castanheira, B. G., & Kepler, S. O. 2008, *MNRAS*, 385, 430
- . 2009, *MNRAS*, 396, 1709
- Chang, H. K., Shih, I. C., Liu, C. Y., et al. 2013, *A&A*, 558, A63
- Choi, J., Dotter, A., Conroy, C., et al. 2016, *ApJ*, 823, 102
- Córscico, A. H., & Althaus, L. G. 2014, *A&A*, 569, A106
- Dolez, N., & Vauclair, G. 1981, *A&A*, 102, 375
- Efron, B. 1979, *Ann. Statist.*, 7, 1
- Ferguson, J. W., Alexander, D. R., Allard, F., et al. 2005, *ApJ*, 623, 585
- Fitzpatrick, E. L. 1999, *PASP*, 111, 63
- Fontaine, G., & Brassard, P. 2008, *PASP*, 120, 1043
- Giammichele, N., Charpinet, S., Fontaine, G., & Brassard, P. 2017, *ApJ*, 834, 136
- Giammichele, N., Fontaine, G., Brassard, P., & Charpinet, S. 2016, *ApJS*, 223, 10
- Giammichele, N., Charpinet, S., Fontaine, G., et al. 2018, *Nature*, 554, 73
- Gianninas, A., Curd, B., Fontaine, G., Brown, W. R., & Kilic, M. 2016, *ApJL*, 822, L27
- Green, G. M., Schlafly, E. F., Finkbeiner, D., et al. 2018, *MNRAS*, 478, 651
- Grevesse, N., & Sauval, A. J. 1998, *SSRv*, 85, 161
- Handler, G., Pikall, H., O'Donoghue, D., et al. 1997, *MNRAS*, 286, 303
- Hansen, C. J., Winget, D. E., & Kawaler, S. D. 1985, *ApJ*, 297, 544
- Hermes, J. J., Montgomery, M. H., Winget, D. E., et al. 2012, *ApJL*, 750, L28
- Hermes, J. J., Montgomery, M. H., Winget, D. E., et al. 2013a, *ApJ*, 765, 102
- Hermes, J. J., Montgomery, M. H., Gianninas, A., et al. 2013b, *MNRAS*, 436, 3573
- Iglesias, C. A., & Rogers, F. J. 1993, *ApJ*, 412, 752
- Iglesias, C. A., & Rogers, F. J. 1996, *ApJ*, 464, 943
- Istrate, A. G., Marchant, P., Tauris, T. M., et al. 2016, *A&A*, 595, A35
- Kawaler, S. D. 1988, in *Advances in Helio- and Asteroseismology*, ed. J. Christensen-Dalsgaard & S. Frandsen, Vol. 123, 329
- Kawaler, S. D. 1993, *ApJ*, 404, 294

- Kawaler, S. D., Bond, H. E., Sherbert, L. E., & Watson, T. K. 1994, *AJ*, 107, 298
- Kilic, M., Hermes, J. J., Gianninas, A., & Brown, W. R. 2015, *MNRAS*, 446, L26
- Kilkenny, D., Welsh, B. Y., Koen, C., Gulbis, A. A. S., & Kotze, M. M. 2014, *MNRAS*, 437, 1836
- Li, Z., Chen, X., Chen, H.-L., & Han, Z. 2019, *ApJ*, 871, 148
- Lin, G., Su, J., Li, Y., & Fu, J. 2021, *ApJ*, 922, 138
- Lopez, I. D., Hermes, J. J., Calcaferro, L. M., et al. 2021, *ApJ*, 922, 220
- O'Donoghue, D. 1994, *MNRAS*, 270, 222
- Panei, J. A., Althaus, L. G., Chen, X., & Han, Z. 2007, *MNRAS*, 382, 779
- Paxton, B., Bildsten, L., Dotter, A., et al. 2011, *ApJS*, 192, 3
- Paxton, B., Cantiello, M., Arras, P., et al. 2013, *ApJS*, 208, 4
- Paxton, B., Marchant, P., Schwab, J., et al. 2015, *ApJS*, 220, 15
- Paxton, B., Schwab, J., Bauer, E. B., et al. 2018, *ApJS*, 234, 34
- Paxton, B., Smolec, R., Schwab, J., et al. 2019, *ApJS*, 243, 10
- Pech, D., & Vauclair, G. 2006, *A&A*, 453, 219
- Pech, D., Vauclair, G., & Dolez, N. 2006, *A&A*, 446, 223
- Pelisoli, I., Kepler, S. O., Koester, D., et al. 2018, *MNRAS*, 478, 867
- Robinson, E. L. 1984, *AJ*, 89, 1732
- Robinson, E. L., Kepler, S. O., & Nather, R. E. 1982, *ApJ*, 259, 219
- Rogers, F. J., & Nayfonov, A. 2002, *ApJ*, 576, 1064
- Saio, H., Winget, D. E., & Robinson, E. L. 1983, *ApJ*, 265, 982
- Silvotti, R., Fontaine, G., Pavlov, M., et al. 2011, *A&A*, 525, A64
- Starrfield, S., Cox, A. N., Hodson, S. W., & Clancy, S. P. 1983, *ApJ*, 269, 645
- Tassoul, M. 1980, *ApJS*, 43, 469
- Thoul, A. A., Bahcall, J. N., & Loeb, A. 1994, *ApJ*, 421, 828
- Townsend, R. H. D., & Teitler, S. A. 2013, *MNRAS*, 435, 3406
- Tremblay, P. E., Gianninas, A., Kilic, M., et al. 2015, *ApJ*, 809, 148
- Winget, D. E., & Kepler, S. O. 2008, *ARA&A*, 46, 157